Robotica (2012) volume 30, pp. 1005–1012. © Cambridge University Press 2011
doi:10.1017/S0263574711001238

A new approach to determine the maximal singularity-free zone of 3-RPR planar parallel manipulator

G. Abbasnejad, H. M. Daniali* and S. M. Kazemi

Department of Mechanical Engineering, Babol University of Technology, P.O. Box 484, Babol, Iran

(Accepted November 10, 2011. First published online: December 5, 2011)

SUMMARY

This paper presents a new algorithm to find the singularity-free cylindrical workspace of parallel manipulators. Because of the limited workspace of parallel manipulators cluttered with different types of singularities, a simple and robust technique to determine continuous singularity-free zones in the workspace of parallel manipulators is required. Here, the largest singularity-free cylinder within the workspace for any prescribed orientation ranging around a reference orientation angle of moving platform is determined. To this end, Particle Swarm Optimization is utilized to find the closest point on the singularity surface to the axis of the cylinder. By implementing the algorithm on 3-RPR planar parallel manipulator, the results show that this algorithm improves the efficiency and leads to significantly larger singularity-free workspace than those reported earlier.

KEYWORDS: Parallel manipulator; Workspace; Singularity-free; Optimization; PSO.

1. Introduction

It is well known that parallel manipulators have the higher payload to weight ratio, higher accuracy, and higher stiffness than their serial counterparts. On the other hand, their principal drawbacks are their limited workspaces cluttered with different types of singularities. In singular configurations either the manipulator gains some uncontrollable degrees of freedom (DOF) or loses some. Since the work environment is cluttered with singularities, there is no guarantee that an undergoing motion is singularity-free and trajectory planning inside the workspace becomes very difficult. Recently, this problem has attracted the attentions of many researchers.[1–5] However, it is desirable to develop an algorithm that can locate singularity-free zones in the workspace.[6]

Arsenault and Boudreau[7] presented a method to synthesize planar parallel manipulator for optimal singularity-free workspace. Using genetic algorithm, architectural parameters of the mechanism are optimized to consider three different design criteria, namely the optimization of the mechanism workspace to approach a prescribed workspace, the maximization of the mechanism's dexterity, and the avoidance of singularities inside the workspace.[7] But as mentioned in ref. [6], the procedure cannot guarantee that the workspace is free of singularities. Yang and O'Brien[8] presented a method for the singularity-free workspace design of a three-legged parallel robot in which singular conditions are described as a set of geometrical parameters of the mechanism. In ref. [9], using mechanisms with variable structures, singularity-free zones in the workspace of the parallel manipulator were optimized. Moreover, the singularity-free zones in the workspace of 3-rapid problem resolution (RPR) parallel manipulator with different systems of actuations were compared for maximum pressure angles. Then a procedure was suggested for determining the optimal system of actuation of parallel manipulator.

Li *et al.*[6] presented an algorithm to determine the maximal singularity-free zones of a 3-RPR planar parallel manipulator. In their work, the largest singularity-free disk centered in an arbitrary point in the x–y positioning workspace was determined such that the disk would be free of singularities for any prescribed orientation ranging around a reference orientation angle of moving platform. However, their procedures yield to a constrained minimization problem, which requires some heavy mathematical computations. Li *et al.*[10] extended the same method to determine the singularity-free zones of the Gough–Stewart platform, and again Tale Masouleh and Gosselin[11] used similar approach for determining singularity-free zones in the workspace of planar 3-PRR parallel manipulator. Although the approach yields to a closed form solution, it is complicated and is not applicable to broad range of problems with arbitrary orientation of the moving platform. Moreover, they considered some simple geometry (i.e., disc for 3-RPR planar parallel manipulator and sphere for the Stewart–Gouph platform), which does not represent the real singularity-free zones for these manipulators. Later, Jiang and Gosselin[12–14] computed the real maximal singularity-free workspace of parallel manipulators around a prescribed point. However, they had to solve the problem numerically.

The maximal singularity-free workspace of the manipulator has been addressed in the literature for a prescribed reference point and reference orientation about which the moving platform has translational and rotational movements. But the singularity-free workspace is not optimum as changing these references may cause a larger singularity-free workspace. In this work Particle Swarm Optimization (PSO) is implemented on the problem. The algorithm presented here leads to more accurate solutions than those reported in ref. [6] and alleviates their drawbacks,

* Corresponding author. E-mail: mohammadi@nit.ac.ir

https://doi.org/10.1017/S0263574711001238 Published online by Cambridge University Press

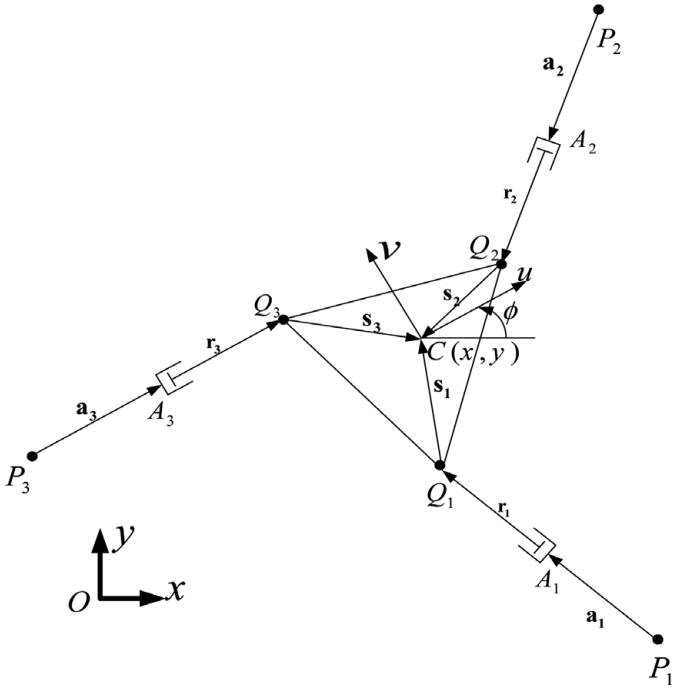


Fig. 1. The geometric model of 3-RPR planar parallel manipulator.

namely heavy mathematical computations. Moreover, the proposed technique can also be easily implemented on other parallel manipulators. At First step, PSO is used to find the closest point on the singularity surface of a 3-RPR planar parallel manipulator to the axis of a cylinder. But this does not lead to the optimal solution, as changing the reference point and reference orientation might lead to different solutions. Therefore, the reference point and reference orientation are improved to extend the singularity-free cylindrical workspace. In order to reveal the efficiency and robustness of the algorithm, the singularity-free workspace presented here will be compared with those reported in the literature.

2. Singularity Surface of 3-RPR Planar Manipulator

The well-known 3-RPR planar parallel manipulator has been studied extensively in the literatures.[6,9,15,16] Here only a brief discussion on the Jacobian matrix and singularity surface of the manipulator is presented. The geometric model of the 3-RPR parallel manipulator is composed of a moving platform and three RPR-type active legs with a prismatic actuators as depicted in Fig. 1. For the sake of analysis, a fixed Cartesian reference coordinate frame $O\{x, y\}$ is fixed to the base at point O, and a moving coordinate frame $C\{u, v\}$ is fixed to the moving platform at point C. Moreover, the parameters x and y represent the absolute coordinates of point C, and ϕ represents its orientation angle.

The velocity for point C is written as follows:

$$\dot{\mathbf{c}} = \dot{\mathbf{a}}_i + \dot{\mathbf{r}}_i + \dot{\mathbf{s}}_i,\ i = 1, 2, 3, \tag{1}$$

where $\dot{\mathbf{a}}_i$, $\dot{\mathbf{r}}_i$, and $\dot{\mathbf{s}}_i$ are given as follows:

$$\begin{aligned} \dot{\mathbf{a}}_i &= \dot{\theta}_i \mathbf{E}\mathbf{a}_i, \\ \dot{\mathbf{r}}_i &= \dot{\gamma}_i \left(1/\left\|\mathbf{r}_i\right\|\right) \mathbf{r}_i + \dot{\theta}_i \mathbf{E}\mathbf{r}_i, \\ \dot{\mathbf{s}}_i &= \dot{\phi}\mathbf{E}\mathbf{s}_i, \end{aligned} \tag{2}$$

in which $\mathbf{a}_i$, $\mathbf{r}_i$, and $\mathbf{s}_i$ are the vectors directed from P_i to A_i, from A_i to Q_i, and from Q_i to C, respectively. Moreover, $\dot{\theta}_i$ is the rate of the first revolute joint of ith leg, $\dot{\gamma}_i$ is the rate of ith prismatic actuator, and $\mathbf{E}$ is the 2×2 orthogonal matrix rotating vector in plane through an angle of 90° counterclockwise, i.e.,

$$\mathbf{E} \equiv \begin{bmatrix} 0 & -1 \\ 1 & 0 \end{bmatrix}.$$

Substituting the values of $\dot{\mathbf{a}}_i$, $\dot{\mathbf{r}}_i$, and $\dot{\mathbf{s}}_i$ from Eq. (2) into Eq. (1), upon simplification leads to

$$\dot{\theta}_i \mathbf{E}(\mathbf{a}_i + \mathbf{r}_i) + \dot{\gamma}_i \left(1/\left\|\mathbf{r}_i\right\|\right) \mathbf{r}_i + \dot{\phi}\mathbf{E}\mathbf{s}_i - \dot{\mathbf{c}} = 0. \tag{3}$$

Upon multiplication of the two sides of Eq. (3) by $(\mathbf{a}_i + \mathbf{r}_i)^T$ to eliminate $\dot{\theta}_i$, associated with an unactuated joint, and writing it in matrix form, one obtains

$$\mathbf{J}\dot{\gamma} + \mathbf{K}\mathbf{t} = 0, \tag{4}$$

where

$$\mathbf{J} = \begin{bmatrix} \left(1/\left\|\mathbf{r}_1\right\|\right)(\mathbf{a}_1 + \mathbf{r}_1)^T r_1 & 0 & 0 \\ 0 & \left(1/\left\|\mathbf{r}_2\right\|\right)(\mathbf{a}_2 + \mathbf{r}_2)^T \mathbf{r}_2 & 0 \\ 0 & 0 & \left(1/\left\|\mathbf{r}_3\right\|\right)(\mathbf{a}_3 + \mathbf{r}_3)^T \mathbf{r}_3 \end{bmatrix},$$

$$\mathbf{K} = \begin{bmatrix} (\mathbf{a}_1 + \mathbf{r}_1)^T \mathbf{E}\mathbf{s}_1 & -(\mathbf{a}_1 + \mathbf{r}_1)^T \\ (\mathbf{a}_2 + \mathbf{r}_2)^T \mathbf{E}\mathbf{s}_2 & -(\mathbf{a}_2 + \mathbf{r}_2)^T \\ (\mathbf{a}_3 + \mathbf{r}_3)^T \mathbf{E}\mathbf{s}_3 & -(\mathbf{a}_3 + \mathbf{r}_3)^T \end{bmatrix}, \dot{\gamma} = \begin{bmatrix} \dot{\gamma}_1 \\ \dot{\gamma}_2 \\ \dot{\gamma}_3 \end{bmatrix}, \mathbf{t} = \begin{bmatrix} \dot{\phi} \\ \dot{\mathbf{c}} \end{bmatrix}.$$

Considering Eq. (4), three types of singularities can be identified for parallel manipulators.[17,18] Singularities of type I, which are usually located at the boundaries of the workspace of the manipulator, occur when matrix $\mathbf{J}$ is singular. These singularities lead to simple expressions and are easily avoided.[6,17] Singularities of type II occur when matrix $\mathbf{K}$ is singular. These singularities usually occur within the workspace in which the manipulator gains one or more uncontrollable DOF, therefore they should be avoided. Singularities of type III occur when both matrices $\mathbf{J}$ and $\mathbf{K}$ are singular simultaneously. For 3-RPR planar parallel manipulator, this type of singularity does not occur.[6]

The condition for the second type of singularity, namely $\mathrm{Det}(\mathbf{K}) = 0$ leads to

$$F(x, y, \phi) = 0, \tag{5}$$

where F is a quartic function of $x, y, \cos(\phi)$ and $\sin(\phi)$. This singularity surface can be plotted for a given ranges of

https://doi.org/10.1017/S0263574711001238 Published online by Cambridge University Press

Table I. Architecture parameters of 3-RPR parallel manipulator.

i	P_i(mm)	Q_i^C(mm)
1.	$[3.78, 4.34]^T$	$[-4.38, -3.19]^T$
2.	$[34.47, -3.78]^T$	$[12.04, -3.19]^T$
3.	$[16.23, 34.76]^T$	$[8.23, 12.09]^T$

x, y, ϕ. Here, we use the data as studied in ref. [6] and given in Table. I. The singularity surface is plotted for two different ranges as depicted in Fig. 2.

3. Overview of Particle Swarm Optimization

Particle Swarm Optimization as an algorithm inspired by the social behavior of flocking animals, such as swarms of birds, ants, and fish school, was first developed and introduced by Kennedy and Eberhart[19] and has been found to be useful in a wide variety of optimization problems. Examples of successful applications of PSO on the issue of manipulator optimal design can be found in refs. [20–22]. In this algorithm, a swarm of m individuals called "particles" is exploited to probe in an n-dimensional search space. Each particle moves in the search space by adjusting their position according to the best position encountered by themselves and their neighbors during the procedure. To have a brief discussion on the algorithm, let the ith particle be represented as $\boldsymbol{\chi}_i = [\chi_{i1}, \chi_{i2}, \chi_{ij}..., \chi_{in}]^T$ and the velocity of this particle be denoted as $\boldsymbol{v}_i = [v_{i1}, v_{i2}, ..., v_{in}]^T$. The best position (the position giving the best fitness value) of the ith particle is recorded and represented as $\mathbf{p}_i = [p_{i1}, p_{i2}, ..., p_{in}]^T$, which is called *pbest*, and the global best position obtained so far by any particle of the swarm is called *gbest* and is represented by the subscript g. Then the concept of the algorithm consists of adapting the velocity and position of the particles in each time step according to the following equations:

$$\boldsymbol{v}_i(k+1) = \omega \times \boldsymbol{v}_i(k) + c_1 \times \text{rand}_1 \times (\mathbf{p}_i(k) - \boldsymbol{\chi}_i(k)) + c_2 \times \text{rand}_2 \times (\mathbf{p}_g(k) - \boldsymbol{\chi}_i(k)), \quad (6)$$

$$\boldsymbol{\chi}_i(k+1) = \boldsymbol{\chi}_i(k) + \boldsymbol{v}_i(k+1), \quad (7)$$

where ω is the inertia weight, c_1 and c_2 represent positive acceleration constants, k is the iteration counter, and rand_1 and $\text{rand}_2 \in [0, 1]$ are uniformly distributed random numbers. The first term in Eq. (6) relates to the current velocity of the swarm, the second term represents the local search, while the third one represents the global search pointing toward the optimal solution.

4. Singularity-Free Cylindrical Workspace

The singularity-free zones in the workspace are cylinder centered in $[x_0, y_0]$ around which the moving platform moves without any singularity for any orientation of the platform ranging within $[\phi_{\min}, \phi_{\max}]$. In this paper the cylinder center and the angle $\phi_{\min}$ are defined as the center point and the reference orientation angle about which the moving platform moves and orientates. Now the problem can be simplified as finding the maximum radius of the singularity-free cylinder. To this end, the closest point on the singularity surface with ϕ ranging within $[\phi_{\min}, \phi_{\max}]$ to the center point is calculated. As a matter of fact, we are looking for three variables x, y, ϕ constrained with Eq. (5) such that the square of the distance of $[x, y]$ to the center point $[x_0, y_0]$ is minimal, i.e., $\min d = (x - x_0)^2 + (y - y_0)^2$ is constrained to

$$F(x, y, \phi) = 0. \quad (8)$$

To solve this optimization problem, PSO algorithm searches in two-dimensional $y - \phi$ space. Choosing the two variables y, ϕ and the architecture parameters of the mechanism, the constraint equation F reduces to a quadratic polynomial in x. Upon solving the polynomial for x, the closest point on the singularity surface to the center point can be calculated. The flowchart of the algorithm is summarized in Fig. 3.

5. Case Studies

Here we use the foregoing algorithm to find the largest cylindrical singularity-free workspace of 3-RPR planar parallel manipulator. By decreasing the inertia weight from

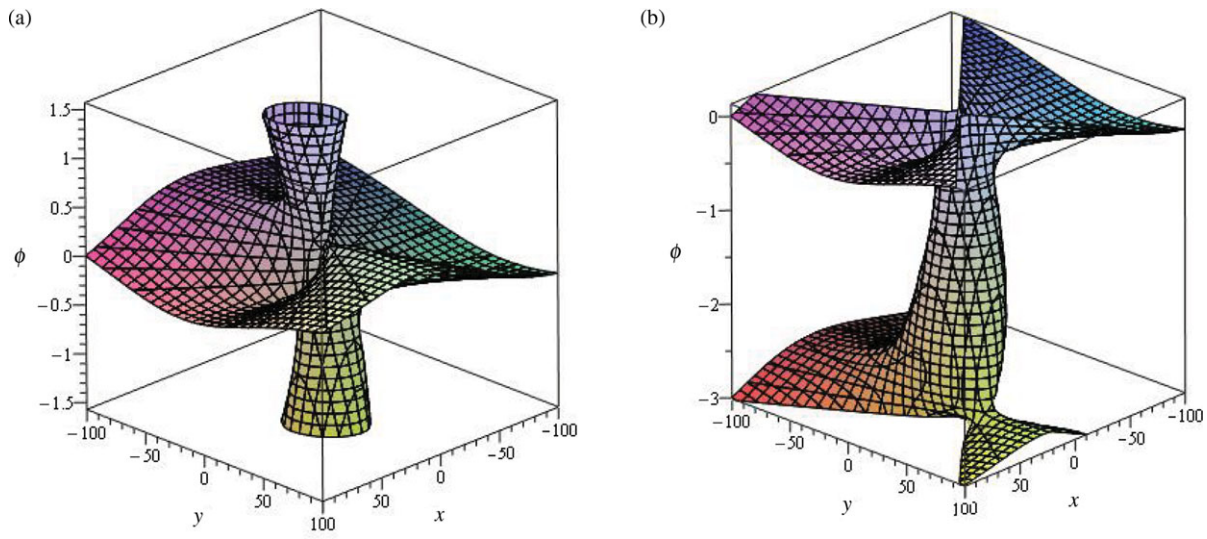


Fig. 2. (Colour online) Singularity surface of 3-RPR mechanism. (a) $-100 < x$ (mm) < 100, $-100 < y$ (mm) < 100, $-\pi/2 < \phi$ (rad) $< \pi/2$; (b) $-100 < x$ (mm) < 100, $-100 < y$ (mm) < 100, $-3.0106 < \phi$ (rad) < 0.1310.

https://doi.org/10.1017/S0263574711001238 Published online by Cambridge University Press

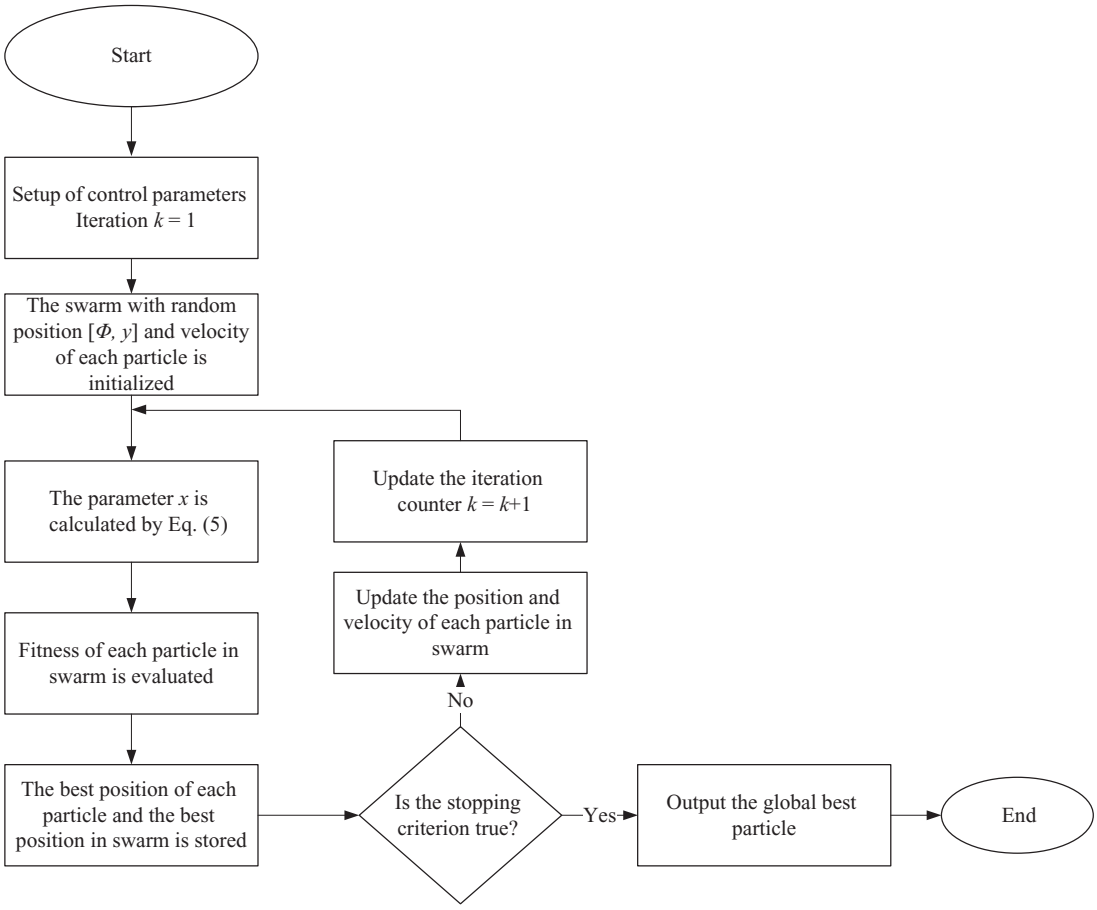


Fig. 3. Flowchart of PSO algorithm.

a relatively large value to a small value, the PSO algorithm tends to have more global search ability at the beginning while having more local search ability near end of the run.[23] Here a gradually decreasing inertia weight value from 0.4 to 0.1 with a linear decreasing rate as a function of number of iteration is used. According to our experiences, the algorithm results the best when the value of acceleration constants C_1 and C_2 are set to 3.5 and 0.5, respectively. A more detailed analysis of the effect of C_1 and C_2 on the sensitivity of the parameters in the optimization problem can be found in ref. [24]. Also, the population size in all examples is set to 70 iterations and the stop criterion is chosen as 100 iterations.

In order to verify the accuracy of the algorithm, the architecture parameters are adopted here as same as in ref. [6],

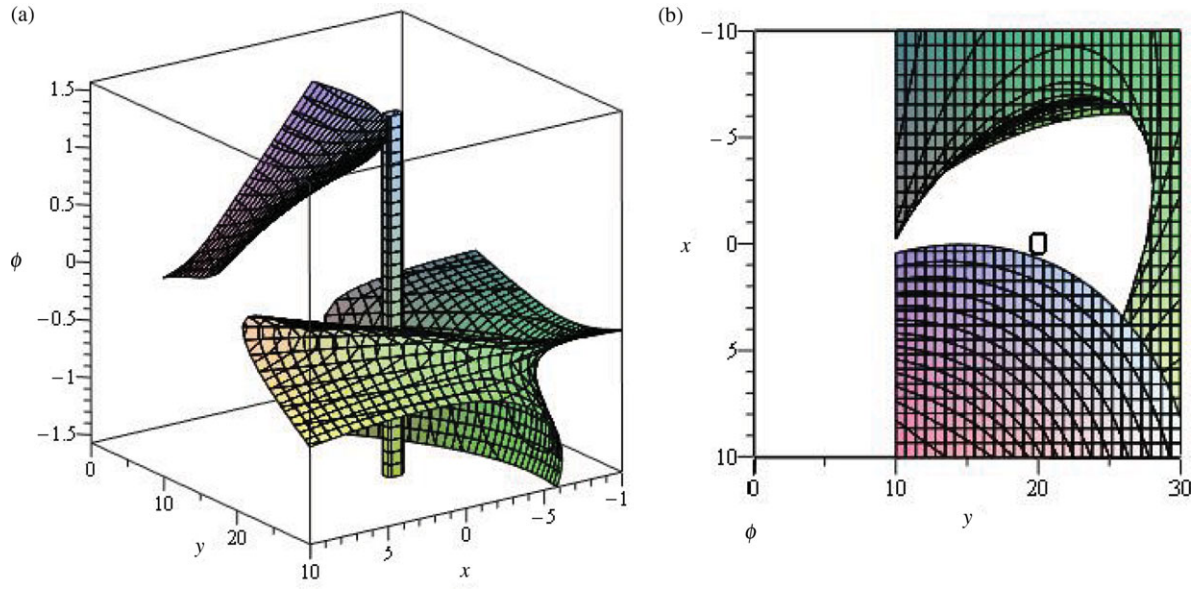


Fig. 4. (Colour online) (a) Maximal singularity-free cylinder with $\phi \in [-\frac{\pi}{2}, \frac{\pi}{2}]$rad; (b) top view of singularity-free cylinder.

https://doi.org/10.1017/S0263574711001238 Published online by Cambridge University Press

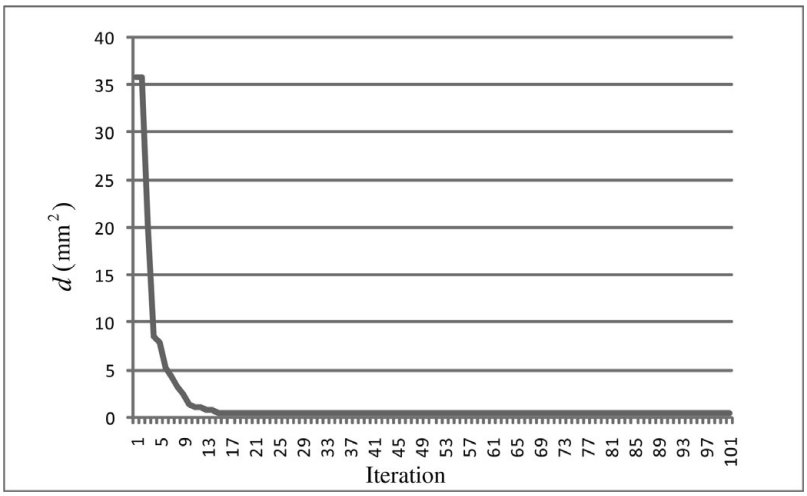


Fig. 5. Convergence pattern of PSO for case 1.

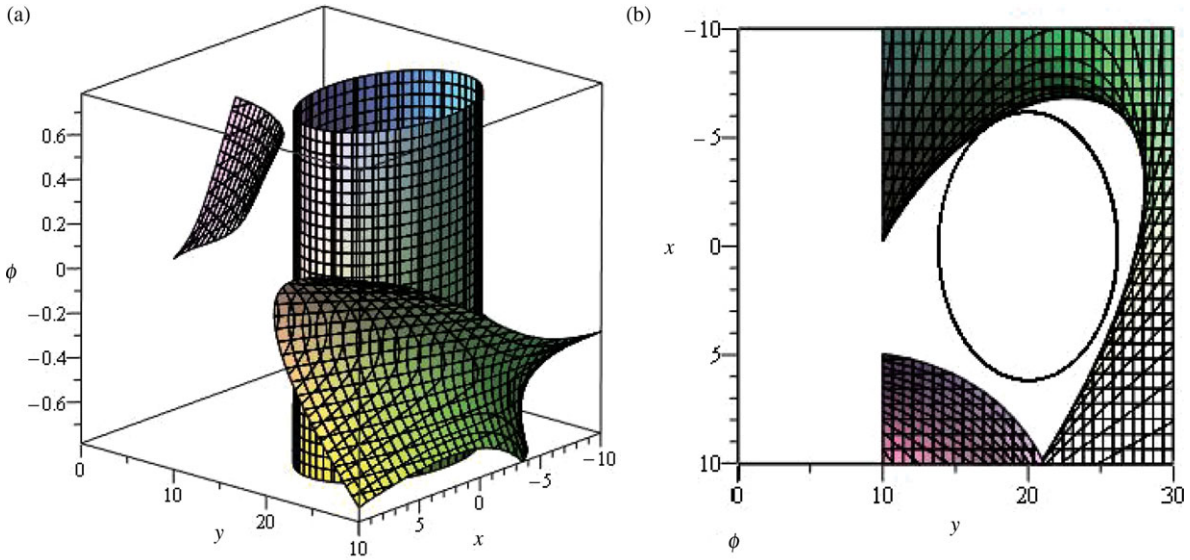


Fig. 6. (Colour online) (a) Maximal singularity-free cylinder with $\phi \in [-\frac{\pi}{4}, \frac{\pi}{4}]$rad; (b) top view of singularity-free cylinder.

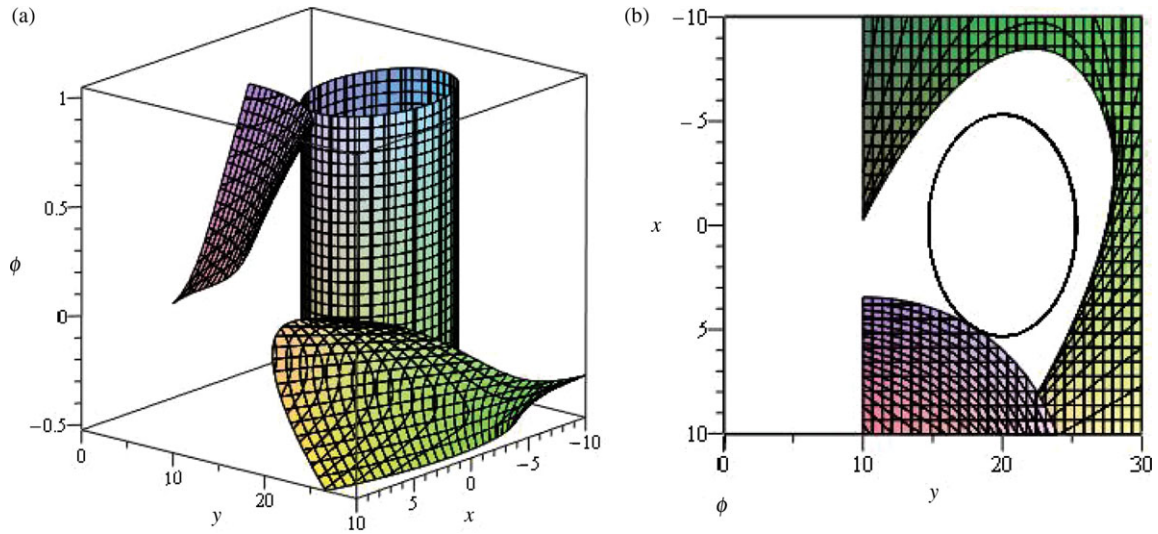


Fig. 7. (Colour online) (a) Maximal singularity-free cylinder with $\phi \in [-\frac{\pi}{6}, \frac{\pi}{3}]$rad; (b) top view of singularity-free cylinder.

https://doi.org/10.1017/S0263574711001238 Published online by Cambridge University Press

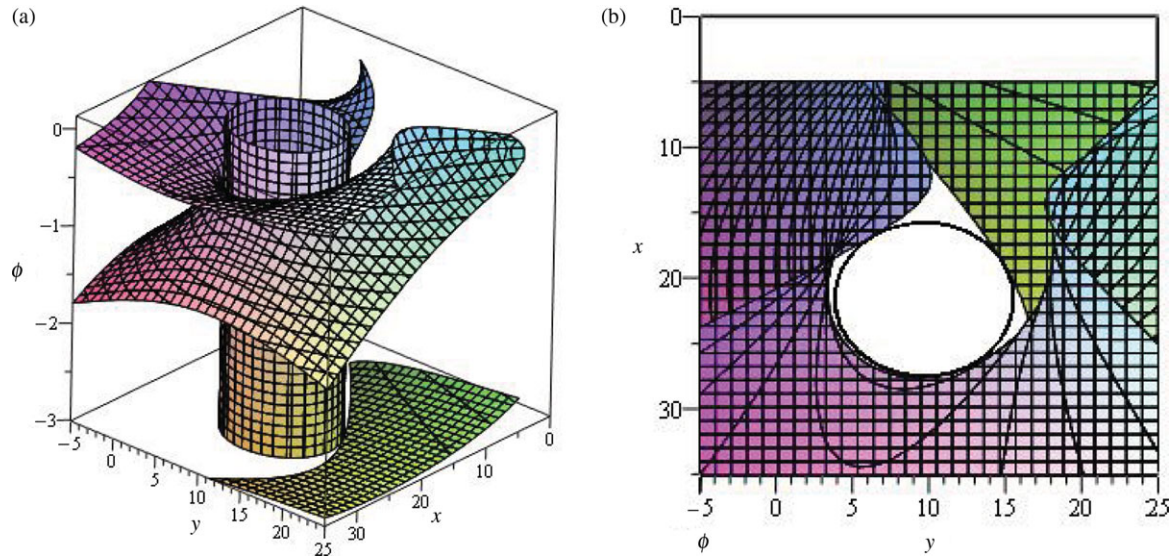


Fig. 8. (Colour online) (a) Extended maximal singularity-free cylinder with $\phi \in [-3.0106,\ 0.1310]$ rad; (b) top view of singularity-free cylinder.

which are given in Table I, and with the same center point, namely [0, 20].

First, the range of moving platform orientation is set to $[-\frac{\pi}{2}, \frac{\pi}{2}]$rad. Then the algorithm leads to $d = 0.4387\,\text{mm}^2$ as the maximal singularity-free cylindrical workspace, which is the same as reported in ref. [6]. The singularity surface and the related singularity-free cylinder with the center point [0, 20] are shown in Fig. 4.

Moreover, the convergence pattern of the algorithm for this example is shown in Fig. 5, which shows very fast convergence. However, it is obvious from Fig. 4(b) that one can reach to a much bigger singularity-free cylinder by changing the center point. It is noteworthy that the method given in ref. [6] does not have this flexibility.

In the next case the moving platform orientation range is reduced to $[-\frac{\pi}{4}, \frac{\pi}{4}]$rad. Calculation of the singularity-free cylinder leads to $d = 38.1859\,\text{mm}^2$, which is larger than $d = 21.5991\,\text{mm}^2$ as reported in ref. [6]. To verify the accuracy of the result, the singularity surface and the related singularity-free cylinder are plotted in Fig. 6. Again, it is obvious from Fig. 5(b) that one can reach to a larger singularity-free cylinder by changing the center point of the cylinder.

The other advantage of the present algorithm is its flexibility in considering different ranges of moving platform orientations. In order to illustrate this, in the following example an unsymmetrical ranges for orientation, namely $[-\frac{\pi}{6}, \frac{\pi}{3}]$rad, is considered. The maximal singularity-free cylinder leads to $d = 28.3031\,\text{mm}^2$ as shown in Fig. 7.

Fast running time is another advantage of the present algorithm. The running times of the algorithm for all the above examples are less than 1 s, while solving the same problems with the method presented in ref. [6] it takes 2 min.

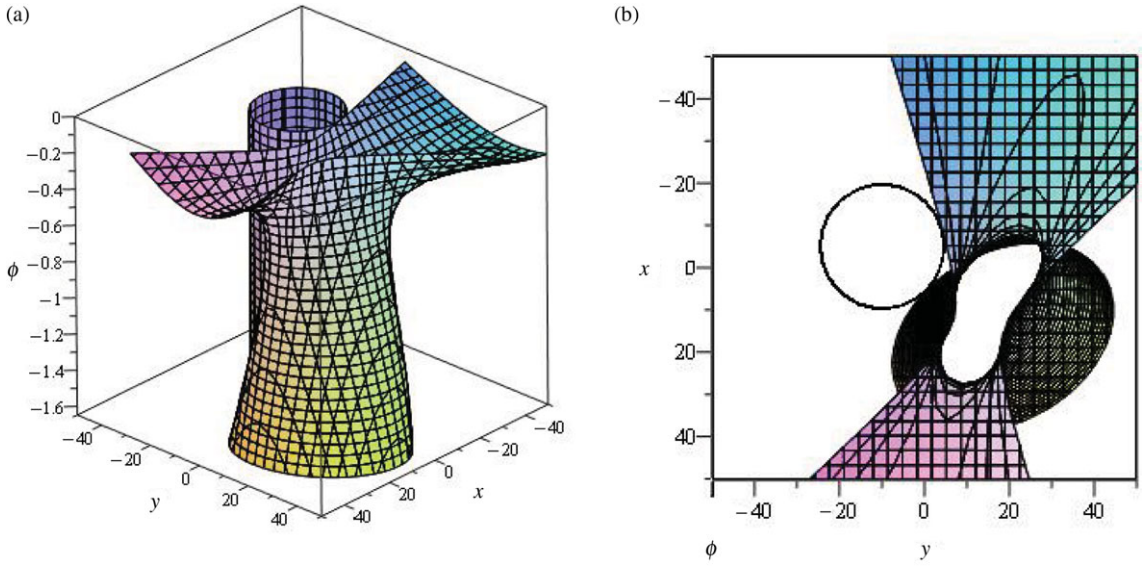


Fig. 9. (Colour online) (a) Extended maximal singularity-free cylinder with $\phi \in [-1.6470,\ -0.07620]$ rad; (b) top view of singularity-free cylinder.

https://doi.org/10.1017/S0263574711001238 Published online by Cambridge University Press

Table II. Results of the center points and reference orientation angles optimization.

Orientation range (rad)	Optimized center points (x_0, y_0) mm	Optimized reference angles $\phi_{\min}$(rad)	Our method d^2(mm^2)	Method of ref. [6] d^2(mm^2)	Increased percentage
π	(21.6144, 9.6967)	−3.0106	34.5313	0.4387	7771.27%
$\pi/2$	(−5, −10)	−1.6470	216.1762	38.1859	466.11%

6. Extended Singularity-Free Cylindrical Workspace

As explained earlier, the singularity-free zone is defined as a cylinder centered in a point in the *x--y* plane, which is singularity-free for a given orientation rages of the moving platform. Both Figs. 2(a) and (b) show the singularity surfaces of the mechanism with the same orientation ranges of moving platform, i.e., $\Delta\phi = \pi$ rad, but with different reference orientation angles. According to Fig. 2(a) the reference orientation angle is zero and the platform is allowed to orientate within $[-\frac{\pi}{2}, \frac{\pi}{2}]$rad, while in Fig. 2(b) the platform is allowed to orientate within $[-3.0106, 0.1310]$rad. It is obvious that one can inscribe a larger cylinder in Fig. 2(b) than in Fig. 2(a). This will be illustrated by the following example. Moreover, as explained earlier, one might reach to bigger singularity-free cylinders by changing the positions of their axes. So it can be concluded that for a given range of the moving platform orientation, $\Delta\phi$, the size of singularity-free cylinders can be increased by changing the center point and reference orientation angle. Here the PSO algorithm is again implemented for the optimal singularity-free cylinder. Now the algorithm is searching in 3-D space, namely in $[x_0, y_0, \phi_{\min}]$, in order to maximize the minimum distance from the singularity surface to the axis passing through $[x_0, y_0]$ for a given ranges of $\Delta\phi$. So, for any guess of $\phi_{\min}$ the moving platform is limited within the range of orientation $[\phi_{\min}, \phi_{\min} + \Delta\phi]$. The architecture parameters chosen are the same as those given in the last section. In order to find a feasible value of the parameters x_0, y_0, within the workspace of the mechanism the search domain is constrained as

$$-5\,\text{mm} < x_0 < 35\,\text{mm},$$
$$-10\,\text{mm} < y_0 < 30\,\text{mm}.$$

In order to show the efficiency of the algorithm, the singularity-free cylinder is optimized for two different ranges of orientation angles. The optimal results are given in Table II and compared with those reported by the other study.[6] For the range of $\Delta\phi = \pi$ the singularity-free cylinder according to our method, as shown in Fig. 7, is 7771% bigger than that based on the method reported in ref. [6]. For the range of $\Delta\phi = \pi/2$ the cylinder based on this algorithm, as shown in Fig. 8, is 466% bigger than that of reported earlier. Moreover, as it is illustrated in Fig. 9, the singularity-free cylinder can be placed inside or outside the singularity surface.

7. Conclusion

In this paper, PSO has been implemented for the calculation of maximal singularity-free cylindrical workspace of 3-RPR planar parallel manipulator. The largest singularity-free cylinder within the workspace for any prescribed orientation ranging around a reference orientation angle of the moving platform has been determined. To this end, PSO has been utilized to find the closest point on the singularity surface to the axis of the cylinder. Numerical examples were included, which demonstrated the efficiency of the algorithm and lead to significantly larger workspace than those reported earlier.

References

1. J. P. Merlet, "Trajectory verification in the workspace for parallel manipulators," *Int. J. Robot. Res.* **13**(4), 326–333 (1994).
2. S. Bhattacharya, H. Hatwal and A. Ghosh, "Comparison of an exact and an approximate method of singularity avoidance in platform-type parallel manipulators," *Mech. Mach. Theory* **33**, 965–974 (1998).
3. S. Ambike and J. P. Schmiedeler, "A methodology for implementing the curative theory approach to path tracking with planar robots," *Mech. Mach. Theory* **43**, 1225–1235 (2008).
4. A. K. Dash, I. M. Chen, S. H. Yeo and G. Yang, "Singularity-Free Path Planning of Parallel Manipulators using Clustering Algorithm and Line Geometry," **In**: *Proceedings of IEEE International Conference on Robotics and Automation (ICRA 2003)*, Taipei, Taiwan (Sep. 2003) pp. 14–19.
5. S. Seyyedi Parsa, H. M. Daniali and R. Ghaderi, "Optimization of parallel manipulator trajectory for obstacle and singularity avoidances based on neural network," *Int. J. Adv. Manuf. Tech.* **51**(5–8), 811–816 (2010). DOI:10.1007/s00170-010-2644-0
6. H. Li, C. M. Gosselin and M. J. Richard, "Determination of maximal singularity-free zones in the workspace of planar three-degree-of-freedom parallel mechanisms," *Mech. Mach. Theory* **41**, 1157–1167 (2006).
7. M. Arsenault and R. Boudreau, "The synthesis of three-degree-of-freedom planar parallel mechanisms with revolute joints (3-RRR) for an optimal singularity-free workspace," *J. Robot. Syst.* **21**(5), 259–274 (2004).
8. Y. Yang and J. F. O'Brien, "A sequential method for the singularity-free workspace design of a three-legged parallel robot," *Mech. Mach. Theory* **45**, 1694–1706 (2010).
9. V. Arakelian, S. Briot and V. Glazunov, "Increase of singularity-free zones in the workspace of parallel manipulators using mechanisms of variable structure," *Mech. Mach. Theory* **43**(9), 1129–1140 (2008).
10. H. Li, C. M. Gosselin and M. J. Richard "Determination of the maximal singularity-free zones in the six-dimensional workspace of the general Gough–Stewart platform," *Mech. Mach. Theory* **42**, 497–511 (2007).
11. M. T. Masouleh and C. Gosselin, "Determination of singularity-free zones in the workspace of planar 3-PRR parallel mechanisms," *J. Mech. Des.* (ASME) **129**, 649–652 (2007).
12. Q. Jiang and C. M. Gosselin, "The maximal singularity-free workspace of the Gough–Stewart platform for a given orientation," *J. Mech. Des.* (ASME) **130**, 112304–112308 (2008).
13. Q. Jiang and C. M. Gosselin, "Determination of the maximal singularity-free orientation workspace for the Gough–Stewart platform," *Mech. Mach. Theory* **44**, 1281–1293 (2009).
14. Q. Jiang and C. M. Gosselin, "Geometric synthesis of planar 3-RPR parallel mechanisms for singularity-free workspace", *Tran. CSME* **33**(4), 667–678 (2010).

https://doi.org/10.1017/S0263574711001238 Published online by Cambridge University Press

15. C. L. Collins, J. M. Mccarthy, "The quartic singularity surfaces of planar platforms in the Clifford algebra of the projective plane," *Mech. Mach. Theory* **33**(7), 931–944 (1998).
16. C. Gosselin and J. Angeles, "The optimum kinematic design of a planar three-degree-of-freedom parallel manipulator," *J. Mech. Transm. Autom. Des.* **110**, 35–41 (1998).
17. H. R. Mohammadi Daniali, P. J. Zsombor-Murray and J. Angeles,"Singularity analysis of planar parallel manipulators," *Mech. Mach. Theory* **30**(5), 665–678 (1995).
18. C. Gosselin and J. Angeles, "Singularity analysis of closed-loop kinematic chains," *IEEE Trans. Robot. Autom.* **6**(3), 281–290 (1990).
19. J. Kennedy and R. Eberhart, "Particle Swarm Optimization," **In**: *Proceedings of IEEE International Conference on Neural Networks*, Piscataway, NJ, vol. IV (1995) pp. 1942–1948.
20. Q. Xu and Y. Li, "Kinematic analysis and optimization of a new compliant parallel micromanipulator," *Int. J. Adv. Robot. Syst.* **3**(4), 351–358 (2006).
21. Y. Li and Q. Xu, "Design and optimization of an XYZ parallel micromanipulator with flexure hinges," *J. Intell. Robot. Syst.* **55**, 377–402 (2009).
22. G. Abbasnejad, H. M. Daniali and A. Fathi, "Architecture optimization of 4PUS+1PS parallel manipulator," *Robotica* **29**(5), 683–690 (2011). doi:10.1017/S0263574710000500
23. Y. H. Shi and R. C. Eberhart, "Parameter Selection in Particle Swarm Optimization," **In**: *Evolutionary Programming VII*, Lecture Notes in Computer Science, No. 1447 (1998) 591–600.
24. R. E. Perez and K. Behdinan, "Particle swarm approach for structural design optimization," *Comput. Struct.* **85**, 1579–1588 (2007).

https://doi.org/10.1017/S0263574711001238 Published online by Cambridge University Press